The electrochemical response of electrode-attached redox oligonucleotides is governed by low activation energy electron transfer kinetics

Zhiyong Zheng[1], Soo Hyeon Kim[2], Arnaud Chovin[1], Nicolas Clement[2]*, Christophe Demaille[1]*

1 Université Paris Cité, CNRS, Laboratoire d'Electrochimie Moléculaire, F-75013 Paris, France

2 IIS, LIMMS/CNRS-IIS UMI2820, The Univ. of Tokyo; 4-6-1 Komaba, Meguro-ku Tokyo, 153-8505, Japan

ABSTRACT: The mechanism responsible for electron transport within layers of redox DNA anchored to electrodes has been the subject of numerous studies over the last twenty years, but remains a controversial issue. Herein, we thoroughly study the electrochemical behavior of a series of short, model, ferrocene (Fc) end-labeled dT oligonucleotides, terminally attached to gold electrodes, using high scan rate cyclic voltammetry complemented by molecular dynamics simulations reproducing DNA Brownian motion. We evidence that the electrochemical response of both single-stranded and duplexed oligonucleotides is controlled by the kinetics of electron transfer at the electrode, obeying Marcus theory, but with reorganization energies considerably lowered by the attachment of the ferrocene to the electrode via the flexible DNA chain. This so far unreported effect, that we attribute to a slower relaxation of water around Fc when attached to moving DNA, is shown to uniquely shape the time-dependent electrochemical response of Fc-DNA strands and, being markedly dissimilar for single-stranded and duplexed DNA, likely contributes to the signaling mechanism of E-DNA sensors.

Electrochemical conformational DNA sensors (E-DNA sensors) are sensitive, selective and versatile modern analytical devices.[1–5] They use short DNA strands (oligonucleotides) attached at one end to an electrode, and carrying a redox label at their other end, as sensing elements. Molecular recognition of target molecules dispersed in solution by the anchored redox DNA modulates the electrochemical response of the sensor, and this modulation is used to report the presence of the sought molecules and quantify their concentration. The versatility of E-DNA sensors stems from the ability of oligonucleotides to specifically recognize many different analytes, including complementary DNA strands,[1] small molecules,[6] proteins,[7] viruses,[8] or even living cells.[9,10] In order to optimize the sensitivity of these sensors, it is of utmost importance to understand their signaling mechanism. This means identifying the processes modulating the electrochemical behavior of the strands, among those potentially controlling the rate of electron exchange between the redox label and the electrode.

Of particular interest here are E-DNA sensors using as a sensing elements *dilute* layers of end-grafted, single-stranded, DNA oligonucleotides bearing a redox label which is *not* electronically conjugated to the DNA base stack, nor able to act as an intercalator. This description fits many of E-DNA sensors, and also de facto excludes systems where through-DNA-chain electronic conduction was either evidenced, or can be suspected, as mediating the electron exchange.[11–13] On the contrary, for the DNA systems considered here, a close approach of the redox label to the electrode is required for electron transfer events to occur. As a result, motional dynamics of the chain and electron transfer at the electrode are the two processes potentially kinetically controlling the electrochemical response. Which of these processes is actually rate limiting has been the subject of debate for almost 20 years. [14–22, 23–26]

In early works from our group, fast scan rate cyclic voltammetry (CV) was used to investigate this issue.[14–16] The response of ferrocene (Fc) labeled dT20 chains was analyzed and it was concluded that dynamic bending or rotational motion was governing the CV response of the Fc-$(dT.dA)_{20}$ duplex. Subsequently, Ferapontova et al. studied the behavior of methylene blue (MB- labeled, end-attached DNA duplexes (16-22 bases long) and also observed CV characteristics compatible with diffusional control of the current.[20,23] White et al. reported a similar diffusive-like behavior for end-grafted single-stranded MB-dT_{21} chains.[24] Schuhmann et al. reached similar conclusions for ferrocene-labeled short DNA analogues (peptide nucleic acids, PNA, 3-16 bases long) grafted onto electrodes, from high scan rate cyclic voltammetry studies.[25,26]

In a series of important contributions, Plaxco et al. reported experiments specifically aiming at deciphering the mechanism of electron transport within redox oligonucleotide layers.[19,21,22] They first used alternating current voltammetry (ACV) to study the electrochemical response of MB-labeled, end-attached single-stranded oligo-(dT) nucleotides.[19] Analysis of the ACV data provided an apparent first-order electron transfer rate constant which varied as

the inverse of chain length (i.e. number of dT nucleotides, from 3 to 70). This was interpreted as evidence of the rate of electron transfer controlling the electrochemical signal, on the basis of polymer physics arguments. Later, these authors carried out the same experiments, this time using chronoamperometry as the experimental technique.[21] They then observed an inverse *square* dependence of the apparent electron transfer rate constant on chain length, from which they concluded that it actually was chain dynamics that was the current limiting factor. Shortly after that, they applied the same technique to analyze the response of double-stranded redox DNA and reached the same conclusion.[22]

All of the above works report rate constants, characterizing the electrochemical response of redox-DNA systems, which are in the order of 1-1000 s^{-1}, or apparent diffusion coefficients in the order of 10^{-10} cm^2/s or lower. However, it is striking that these values are orders of magnitude lower than those characterizing the dynamics of short DNA strands free in solution. For example, the translational diffusion coefficient of a single-stranded (ss) 20 bases oligonucleotide is in the order of 10^{-6} cm^2/s.[27] Similarly, a double-stranded (ds) DNA strand of the same length is characterized by a rotational diffusion constant in the order of μs^{-1}.[28,29]

Is also intriguing that, for experiments where anchored oligonucleotides were end-labeled by a fluorophore, and surface-induced fluorescence quenching was used to monitor the motion of the DNA chain, chain dynamics in the expected µs range were systematically observed.[29–31] These fluorescence quenching experiments are comparable to the above-described electrochemical measurements in that they both require the end-label of the DNA chain to approach the anchoring surface within (sub)nanometer distances. The major difference is that in the fluorescence case no electron exchange takes place. One is thus naturally led to wonder whether the particularly slow rate constants measured by electrochemistry do in fact reflect a kinetic control of the signal by the electron transfer step rather than by chain dynamics.

The aim of the present work is to address this question by: (*i*) assembling a model end-grafted redox oligonucleotide system, (*ii*) characterizing its electrochemical response with fast scan rate cyclic voltammetry, and (*iii*) interpreting the results based on a realistic molecular dynamics model for DNA. These simulations, which were previously computationally inaccessible or not quantitative enough, have become possible with the refinement of coarse grained sequence-dependent DNA models such as oxDNA.[32] For the present work, we have developed a code (Qbiol) dedicated to electrochemical application enabling the complete dynamics of the anchored DNA to be numerically reproduced and resolved in time.

We provide evidence here that the electrochemical response of both single-stranded and duplexed redox oligonucleotides is actually kinetically controlled by the electron transfer at the electrode, as described in the framework of Marcus theory,[33–35] but with a reorganization energy considerably lowered by the attachment of the redox label to the flexible DNA chain and to the electrode.

This decrease in reorganization energy drastically changes the electrochemical response of redox DNA strands in a way that can be mistaken for diffusional or elastic bending control. Furthermore, the reorganization energies are found to be markedly dissimilar for ssDNA and dsDNA, a feature which contributes to making hybridization easily detectable by electrochemical measurements, i.e. underlies the signaling mechanism of E-DNA sensors.

Results

Design and assembly of model redox DNA layers

We thoroughly studied the fast scan rate CV response of a series of short, model, poly-(dT) oligonucleotides, labeled at their 3' extremity by a ferrocene redox tag, and 5' end-attached to a gold electrode (Figure 1). Oligonucleotides of sequence dT_N were specifically considered, as these have been preferably used in previous works aiming at characterizing the dynamic behavior of surface-anchored redox-oligonucleotides.[15,16,19,21] In addition, ferrocene was chosen as a redox marker because of its fast and uncomplicated single electron transfer properties. In contrast, methylene blue, often used as a redox label for DNA chains, has a more complex behavior, involving the transfer of 2 electrons and a proton, which interferes with the electrochemical response of the MB-labeled DNA layers.[36]

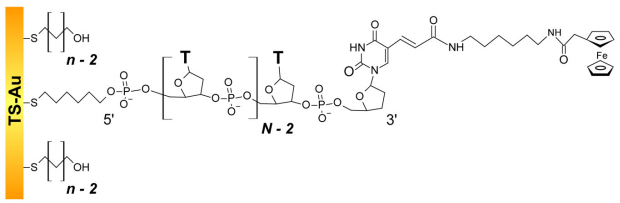

Figure 1. Structure of the dilute ferrocenylated DNA oligonucleotide layers studied in this work. *N* is the number of (dT) nucleotides, *n* the number of CH_2 units of the hydroxyl-terminated alkyl thiol surface diluent.

The length of the oligonucleotides was systematically varied by considering *N* values of 10, 20, 35, and 50. The single-stranded Fc-dT chains (ssDNA) were surface thio-attached to ultra-flat template stripped gold surfaces, via a 6-carbon long, thiol-terminated alkyl linker. Short, hydroxyl-terminated alkyl thiol chains ($HS-(CH_2)_n-OH$) were co-adsorbed with the DNA, to play the role of surface diluent. Formation of such hydrophilic thiol layers also avoids flat-lying adsorption of oligonucleotides.[37,38] Alkyl chains of various lengths, i.e. featuring n = 2, 3, 4, or 6 CH_2, were used. They were chosen so that their length would not exceed that of the C_6 DNA surface linker, and thus allow free

motion of the strand around its 5' end. Co-adsorption of DNA and alkyl thiol was preferred over the more commonly used backfilling of already adsorbed DNA layers, as this was shown to ensure better defined, more homogeneous thiol-DNA layers.[38,39] Besides, by controlling the DNA/alkyl thiol ratio of the adsorption solution, the final Fc-DNA surface concentration could be finely tuned, and its influence on the CV response systematically studied.

We purposefully assembled dilute Fc-DNA layers, characterized by a chain surface concentration in the << 10 pmol/cm² range. Control experiments showed that no chains could be detected on the surface by CV if Fc-dT strands devoid of the thiolated end were used to assemble the layer (Figure S1). We also characterized the structure of the assembled Fc-DNA layer by atomic-force electrochemical microscopy (AFM-SECM). In this technique, a force-sensing microelectrode probe is approached to the surface and used to specifically electrochemically detect the Fc heads of surface-anchored ssDNA chains (see Supporting Information).[40] As can be seen from Figure S2, Fc heads were detected ~5 to ~15 nm *away* from the anchoring gold surface, at distances correlated to the length (*N*) of the ssDNA strands. The above results are a strong indication that the ssDNA chains were properly anchored via their 5' thiol linker, their 3' Fc-labeled end freely exploring a small volume of solution extending from the surface and solely limited by the chain length.

High scan rate CV characterization of end-attached Fc-dT35

Throughout this work, the CV responses of end-anchored DNA layers were recorded in a wide potential scan rate, *v*, region spanning as much as 6 orders of magnitude (0.01 V/s to 10 kV/s), using a high-bandwidth home-designed apparatus. A 1 M ionic strength buffered $NaClO_4$ solution was used as the electrolyte since, at such a high ionic strength, the effect of the electrode electric field on DNA orientation was shown to be vanishingly small.[41]

We first considered Fc-$(dT)_{35}$ layers, formed using mercaptohexanol (n = 6) as a surface diluent. Corresponding typical CV signals recorded at 0.1, 10 and 1000 V/s are shown in Figure 2a, b, c.

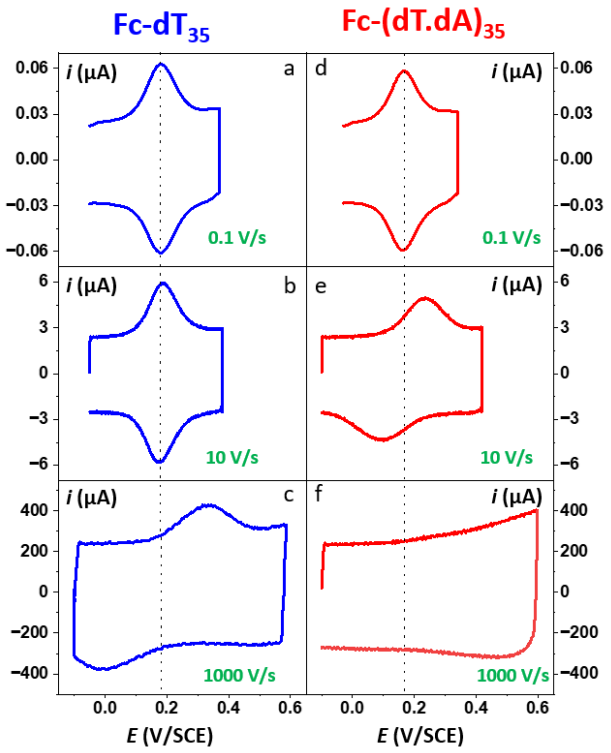

Figure 2. Raw CV signals of electrode end-grafted Fc-DNA recorded at various scan rates. (a,b,c): Single-stranded Fc-dT_{35} chains. (d,e,f): Duplexed Fc-$(dT.dA)_{35}$ chains. The scan rate is indicated in green characters below the CVs. Chain coverage Γ = 5 pmol/cm². Phosphate buffered, 1 M $NaClO_4$ aqueous electrolyte, pH = 7. T= 25°C.

At slow enough scan rates (e.g. 0.1 V/s, Figure 2a), the signal displayed a pair of well-defined, symmetrical current peaks, located at a common peak potential value of ~ 175 ± 3 mV / SCE, corresponding to the standard potential ($E°$) expected for the DNA-borne Fc label used here.[42] The intensity of the (anodic or cathodic) peak current was proportional to the scan rate and the peak full width at mid-height was ~ 97 ± 3 mV. These characteristics are typical of the response of non-interacting surface-attached redox species, located outside the double layer and undergoing fast (Nernstian) electron transfer at the gold electrode. Integration of the charge under the peaks yielded the Fc-ssDNA surface coverage, 5 ± 0.5 pmol/cm², for the CV in Figure 2a, confirming that, under our conditions, dilute ssDNA layers were formed. As the scan rate was raised the peak separation was observed to increase, and the peaks also became relatively broad at high scan rates (Figure 2b, c). A more complete and quantitative description of the changes in signal characteristics with scan rate can be seen in Figure 3, where the variation of the anodic (E_{pa}) and cathodic (E_{pc}) peak positions and of the anodic peak intensity (i_{pa}), normalized by *v*, or by $\sqrt{v}$, are shown in parts a, b, and c, respectively (blue symbols).

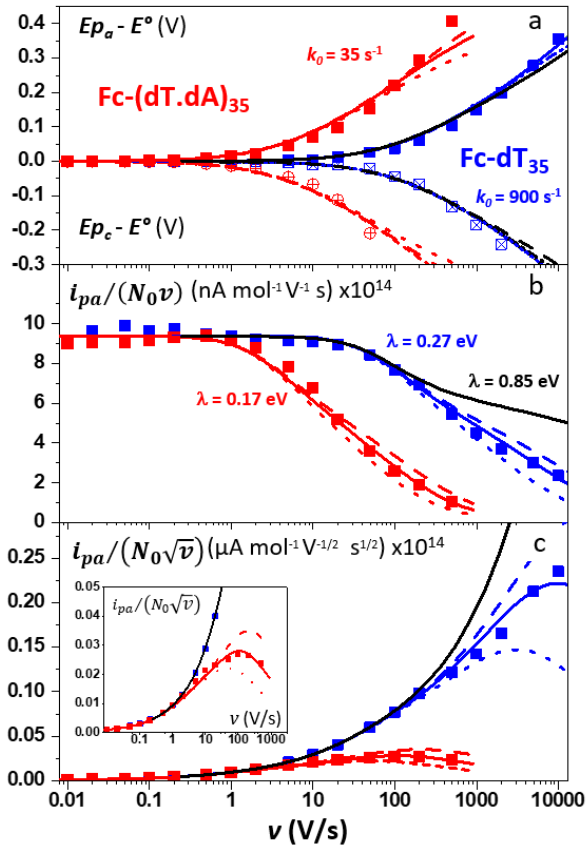

Figure 3. Characteristics of the CV signals of electrode end-grafted Fc-dT$_{35}$ and Fc-(dT.dA)$_{35}$ chains. Variation with the scan rate, v of: (a) Anodic (E_{pa}) and cathodic (E_{pc}) peak potentials expressed vs. the standard potential of the Fc label, $E°$. (b) Anodic peak current, i_{pa}, divided by v, and by the molar number of chains on the surface, N_o. (c) Anodic peak current, i_{pa}, divided by $\sqrt{v}$ and by N_o. The inset is a magnification of the 0.01-1000 V/s region. Solid blue and red lines are fits to the data using the MHL/TLC model, yielding the best fit values of k_o and λ values as indicated in(a) and (b). Dash and dotted red and blue lines were calculated with λ values differing from best-fit values by ± 0.05 eV respectively. The black lines were calculated using k_o = 900 s^{-1} and λ = 0.85 eV. N_o was derived by integration of the slow scan rate CVs. Chain coverage Γ = 5 pmol/cm^2. Phosphate buffered, 1 M $NaClO_4$ aqueous electrolyte, pH = 7. T = 25°C.

It can be seen (in Figure 3a) that, at scan rates above 10 V/s the anodic peak shifted positively while the cathodic peak shifted negatively, so that the peak separation markedly increases, up to more than 0.5 V at 10 kV/s. Such a large increase in peak separation can be attributed to the rate of the electron transfer becoming comparable to the inverse of the CV characteristic "observation" time τ_{cv} = RT/Fv, with F the faraday constant. We note, however, from Figure 3b, that in the same high scan rate region, the i_{pa}/v ratio markedly decreased, while the corresponding ratio $i_{pa}/\sqrt{v}$ increased, without reaching a plateau (Figure 3c). Such behavior is compatible with the ssDNA chain undergoing too-fast-to-be-measured chain dynamics, the system thus behaving as a thin layer cell where a redox species is free to "move" rapidly within a thin layer of solvent confined to the electrode surface.[43,44]

This is to be expected here since, even at the highest scan rate explored of 10 kV/s, τ_{cv} is 2.6 μs, i.e. is approaching but still larger than the expected sub-μs motional time characteristic of (dT)$_{35}$.[29] Such a case is also confirmed by our molecular dynamic simulations reproducing the motion of the anchored chain (*vide infra*).

As discussed by Laviron,[44] in this situation the CV response is expected to be identical to the case of a motionless surface-attached species except that, for simple diffusion, the rate of electron transfer is characterized by a standard first-order rate constant $k_o = k_s/L$, where k_s is the standard heterogeneous electron transfer rate constant of the species and L is the thin layer thickness. In the present case, the motion of the redox label is more complex than simple diffusion, but the equivalence with a motion-less surface species still holds and one can also define a k_o value, proportional to the equilibrium probability of presence of the redox label at the electrode and to k_s (see below).

Moreover, since large overpotential values (E_{pa} - $E°$ and E_{pc} - $E°$) were observed here (Figure 3a), the Marcus-Hush-Levich (MHL) model has to be employed to describe the electron transfer kinetics, rather than the Butler-Volmer model (see Supporting Information).[34,45,46] The MHL model describes the kinetics of electron transfer in terms of two parameters, k_o and λ, the latter being the solvent reorganization energy, which is characteristic of the molecular structure and solvation of the redox probe.[33] In CV the peak separation is only modestly dependent on the λ value,[46–48] so that fitting of the E_{pa} - $E°$ and E_{pc} - $E°$ vs. v variations with the MHL/TLC model can be carried out based on a single adjustable parameter: k_o (see Supporting information- Section 3). For Fc-dT$_{35}$ this yields the best fit value of k_o = 900 ± 100 s^{-1}, Figure 3a, blue traces.

In CV, the peak current is, on the contrary, quite sensitive to the value of λ (see Supporting information- Section 3).[46–48] A λ value of ~ 0.85 eV is reported to be typical for ferrocene species,[34,49–51] both in solution and immobilized on electrodes as redox labels of compact self-assembled thiol layers. We therefore calculated the i_{pa}/v versus scan rate variation expected for this latter λ value using the MHL/TLC model (black line in Figure 3b). As can be seen, this could not account for the sharp decrease of the i_{pa}/v ratio we experimentally observed at high scan rates. However, by using λ as an adjustable parameter (while keeping k_o = 900 s^{-1}), the experimental i_{pa}/v v.s. log v variation could be very satisfyingly reproduced with a best fit value of λ = 0.27 ± 0.03 eV (Figure 3b blue solid line), and so could the $i_{pa}/\sqrt{v}$ variation (Figure 3c). Such a remarkably low λ value seemingly reflects an unexpected effect of the attachment of the ferrocene label to the surface *via* the flexible DNA chain.

Hybridization of the Fc-dT$_{35}$ chain: High scan rate CV characterization of end-attached Fc-(dT.dA)$_{35}$ duplex

The end-anchored, Fc-dT$_{35}$ layer was exposed to fully complementary dA$_{35}$ chains in solution, rinsed with the electrolyte and thoroughly characterized again by high scan rate CV. At slow scan rates, the CV thus obtained was very similar to the one recorded for Fc-dT$_{35}$ (Figure 2d), even showing a similar coverage, indicating the absence of chain loss. The only noticeable difference was that the apparent standard potential of the ferrocene label, $E°$, shifted to a more negative value of $E°$ = 165 ± 3 mV /SCE.

At higher scan rates, the CVs recorded after exposition to dA$_{35}$ differed markedly from those initially recorded for Fc-dT$_{35}$: the peak separation became larger and the peak current lower (Figure 2e). As the scan rate was further raised, the intensity of the peak current relative to the capacitive background decreased, up to the point that, at 1000 V/s and above, the Faradaic signal was no longer discernable, as if "extinct". (Figure 2f).

Such changes in CV signals upon exposing the electrode to dA$_{35}$ are ascribable to the full hybridization of the end-anchored Fc-dT$_{35}$ chain, to form the corresponding Fc-(dT.dA)$_{35}$ duplex. Control experiments showed that when the Fc-dT$_{35}$ layer was exposed to a non-complementary dC$_{35}$ strand in solution its CV characteristics remained unchanged (Figure S3). Besides, simple rinsing with deionized water of the electrode exposed to the dA strand restored the CV characteristics of the Fc-dT layers (Figure S4), as expected from the dehybrization of the duplex in low ionic strength solutions.[52]

The full characteristics of the CV response of the Fc-(dT.dA)$_{35}$ layer are presented in Figure 3 (red symbols). Most notably, upon increasing the scan rate, the peak-to-peak separation increased while the i_{pa}/v ratio decreased, in a similar way than observed for the Fc-(dT)$_{35}$ layer, but from a much lower scan rate threshold of only a few V/s. Interestingly, the $i_{pa}/\sqrt{v}$ ratio passed toward a broad peak (inset in Figure 3c). Such a CV behavior was previously reported by us for Fc-(dT.dA)$_{20}$ layers immobilized on non-MCH treated polycrystalline gold electrodes, and interpreted as a sign of diffusion or elastic rod-bending control of the CV.[15,16] However, we now realize that this behavior can be quantitatively explained by the MHL/TLC model, which, as seen in Figure 3 (red traces), enables the v dependence of the CV characteristics to be perfectly reproduced. This result thus points to fast Fc-(dT.dA)$_{35}$ strand dynamics and to a kinetic control of the CV by the electron transfer rate. Accordingly, our simulations predict that Fc-dsDNA strands undergo fast rotational motions around their anchored 5' end, characterized by times in the ns range, *vide infra*. By contrast, even at the highest scan rate explored for Fc-(dT.dA)$_{35}$ (1000 V/s), τ_{cv} is much larger (26 µs).

Fitting of the peak potentials versus log(v) yielded a best fit k_o value of 35 ± 5 s^{-1} (Figure 3a, red trace). The i_{pa}/v variation could be nicely reproduced using the best fit λ value of 0.17 ± 0.03 eV (Figure 3b). Notably, the peak shape of the experimental $i_{pa}/\sqrt{v}$ vs. v variation could nicely be reproduced by the MHL/TLC model (see inset in Figure 3c), which predicts such shape only for low enough λ values (see Supporting Information – Section 3).

Effect of surface coverage on the CV response of Fc-(dT)$_{35}$ and Fc-(dT.dA)$_{35}$

We next studied systematically the relation between the Fc-DNA coverage on the electrode, Γ, and the CV characteristics. As exemplified in Figure S5, for all of the coverage values explored, the peak potential and peak current variations with scan rate could be very well reproduced using the MHL/TLC model. This yielded sets of k_o, λ values, which are plotted versus the corresponding Γ values in Figure 4, both for Fc-(dT)$_{35}$ and Fc-(dT.dA)$_{35}$ layers.

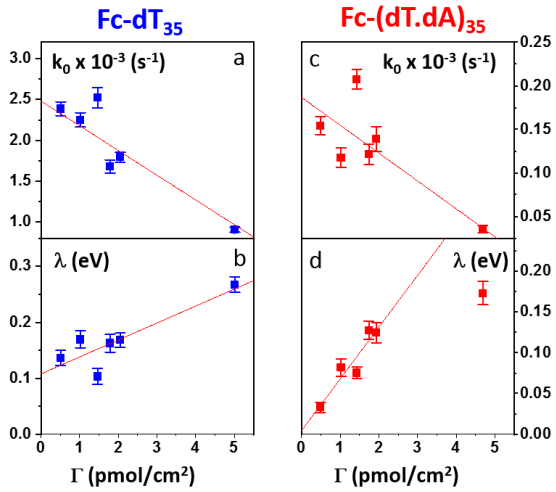

Figure 4. Variation of the kinetic parameters k_o and λ, characterizing the rate of electron transfer of end-anchored Fc-DNA chains, as a function of the chain coverage Γ. (a,b): Single-stranded Fc-dT$_{35}$. (c,d): Hybridized Fc-(dT.dA)$_{35}$. Red lines are guides to the eye. Error bars correspond to 3 times the standard deviation on the best fit values for k_o and λ (see Supporting Information). Phosphate buffered, 1 M $NaClO_4$ aqueous electrolyte, pH = 7. T = 25°C.

One can observe that, in both cases, k_o values are the highest for the lowest coverage values and decrease as Γ is increased (Figures 4a and 4c). Conversely, λ values are seen to increase with increasing Γ (Figures 4b and 4d). For Fc-(dT)$_{35}$ layers, λ increases from a lower value of ~0.13 ± 0.03 eV at low coverage, toward 0.25 ± 0.03 eV at the highest coverage. For the Fc-(dT.dA)$_{35}$ duplex, a vanishingly small λ value of ~0.025 eV is recorded at low Γ, and a 0.17 ± 0.03 eV value at the highest coverage.

Lateral interactions between end-grafted chains are expected to become significant when the average distance between the chains' anchoring points on the surface is lower than their length, L_c. Counting 0.7 nm per nucleotide for ssDNA[53] and 0.34 nm for dsDNA,[54] L_c values of 25 nm and 12 nm, can be estimated for Fc-(dT)$_{35}$ and Fc-(dT.dA)$_{35}$,

respectively. Hence, interactions can become significant if the coverage greatly exceeds a threshold coverage: $\Gamma_i = 1/(\mathcal{N} L_c^2)$, $\mathcal{N}$ being the Avogadro number. Γ_i is equal to 0.3 pmol/cm² for Fc-$(dT)_{35}$ and to 1 pmol/cm² for Fc-$(dT.dA)_{35}$. Since the data presented in Figure 4 cover a Γ range of 0.5 to 5 pmol/cm² we can conclude that the k_o and λ vs Γ variations we measured actually translate the modulation of the electron transfer parameters by lateral interactions between neighboring chains. Note that even at the highest Γ value explored (5 pmol/cm²), the average chain separation is ~6 nm, which is sufficient large to exclude interactions between *the Fc labels* of neighboring chains, since they are much smaller in size (0.27 nm radius).[55] The k_o and λ values measured at the lowest coverage value explored (0.5 pmol/cm²) can reasonably be taken as typical of isolated (non-interacting) chains, whose CV response we primarily intend to model in this work.

Effect of DNA chain length, *N*, on the CV response of Fc-$(dT)_N$ and Fc-$(dT.dA)_N$

As pointed out by Plaxco et al.,[19,21,22] a most important parameter to consider in order to decipher whether chain motion or electron transfer kinetics control the electrochemical response of end-anchored redox-DNA is the DNA chain length, represented here by the number of (dT) nucleotides, *N*. We therefore conducted high scan rate CV characterizations for Fc-dT_N chains, with *N* = 10, 20, 35, and 50, starting with a systemic study of the effect of the chain coverage, Γ (using MCH as a surface diluent, *n* = 6).

In each and every case a very good fit of the CV data with the MHL/TLC model was obtained (Figure S6), from which sets of k_o and λ values could be accurately derived. Decreasing k_o vs. Γ and increasing λ vs. Γ variations were systematically observed for all chain lengths (e.g. Figure S8 and Figure S9).

In any case, the lowest Γ value explored was low enough for the corresponding k_o, λ set of values to be assigned to the behavior of isolated chains. These values are plotted as a function of *N* in Figure 5.

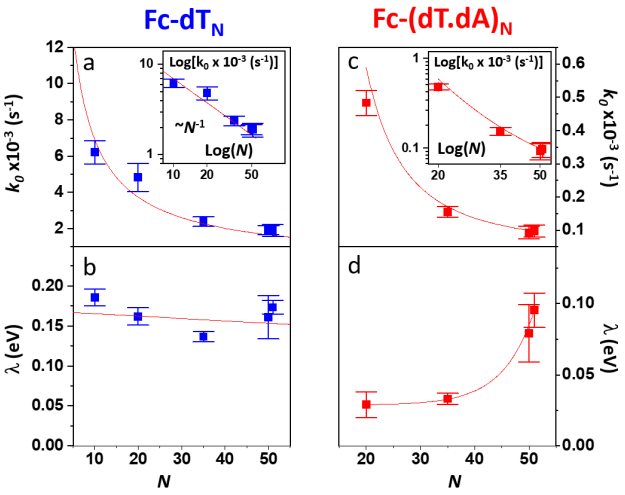

Figure 5. Variation of the kinetic parameters k_o and λ, characterizing the rate of electron transfer of end-anchored Fc-DNA chains, as a function of the DNA chain length, i.e. number of nucleotides *N*. (a,b): Single-stranded Fc-dT_N. (c,d): Hybridized Fc-$(dT.dA)_N$. Red curves in (a), (c) and insets are fits of equation (2) to the data, in (b) and (d) red lines are guides to the eye. Phosphate buffered, 1 M $NaClO_4$ aqueous electrolyte, pH = 7. T = 25°C.

For the single-stranded chains Fc-dT_N, k_o is observed to decrease rapidly with increasing chain length, *N*, (Figure 5a). More precisely, k_o nicely decreased as $1/N$, as seen from the log(k_o) vs log (*N*) plot presented in inset. As shown in Figure 5b, λ values for the Fc-dT_N varied little with increasing *N*.

Measurements were also carried out with the fully hybridized Fc-$(dT.dA)_N$ chains, except for *N* = 10 where hybridization could not be unambiguously evidenced, likely due to a too low melting point of this short duplex. For the Fc-$(dT.dA)_N$ duplexes, k_o was also observed to decrease rapidly with increasing chain length (Figure 5c), while being systematically at least an order of magnitude lower than that for non-hybridized chains. Figure 5d shows that λ increased with *N*, while remaining below ~0.1 eV.

Effect of diluent length, *n*, on the CV response of Fc-$(dT)_{50}$ and Fc-$(dT.dA)_{50}$ layers

The effect of the actual length (i.e. number *n* of CH_2 units) of the alkyl thiol diluent on the CV response of Fc-DNA and Fc-dsDNA was also studied. For this, Fc-$(dT)_{50}$ was thiol-end adsorbed in the presence of an excess of the chosen diluent (*n* = 2, 3, 4 or 6). The final Fc head coverage was kept low enough (i.e. << 1 pmol/cm²) for the Fc-DNA chains to behave as isolated entities. Here again, the MHL/TLC model enabled us to fully account for the CV characteristics of the chains, both single-stranded and duplexed, for all the diluent thiols explored (Figure S7).

The thus derived sets of k_o, λ values were then plotted as a function of *n*, Figure 6.

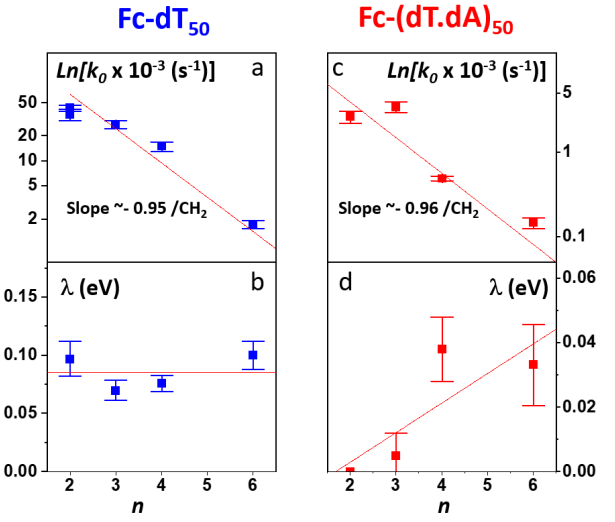

Figure 6. Variation of the kinetic parameters k_o and λ, characterizing the rate of electron transfer of end-anchored Fc-DNA chains, as a function of the length of the alkyl thiol surface diluent, i.e. number of CH_2 units *n*. (a,b): Single-stranded Fc-dT_{50}. (c,d): Hybridized Fc-$(dT.dA)_{50}$. Red lines in (a) and (c) are linear regression lines, in and (b) and (d) they are guides to the eye. Phosphate buffered, 1 M $NaClO_4$ aqueous electrolyte, pH = 7. T = 25°C.

Both for Fc-$(dT)_{50}$ (Figure 6a) and Fc-$(dT.dA)_{50}$ (Figure 6c), k_o was seen to decrease exponentially, with *n*. Such a result is strong evidence that, for our system, electron transfer to the redox Fc heads does not proceed through the DNA chain, since in this case its rate would not be affected by the length of the alkyl thiol diluent. Conversely, such dependence is expected if the electron is transferred by the Fc label to the electrode *through* the diluent layer.

This result falls in line with the dependence of the current on the diluent thickness previous noted for some E-DNA sensors.[56,57]

Turning now to the dependence of λ on *n*, one can observe in Figure 6b, that, for Fc-$(dT)_{50}$, λ remains approximately constant, around a low value of 0.07 eV. For Fc-$(dT.dA)_{50}$, λ values are typically even lower (Figure 6d), going from almost zero for *n* = 2 and increasing to a maximum value of ~0.04 for *n* = 6.

Molecular dynamic simulations of the behavior of end-attached Fc-DNA layers

We have developed a molecular dynamics simulation code (Qbiol), based on the OxDNA package, to resolve the motional dynamics of end-anchored ss and ds FcDNA (see Supporting Information - Section 4). While numerical simulations considering a molecular pendulum (rod with electrostatics) have shown to nicely reproduce the dynamics of protein-binding using double-stranded DNA and a specific antibody,[58] such an approach remains too simple to capture the dynamics of protein-free DNA, and in particular ssDNA that does not behave as a rod. In Qbiol, the 1st base (in 5') is considered as the anchoring site, punctually attached to the surface via a strong elastic force. The position of the Fc head, assumed to correspond to the free 3' end of the DNA, can be tracked for many different configurations with a ~1 ps time step, for periods of 10 μs, using an optimized code (see Supporting Information – Section 4). This enables us to build two-dimensional heat maps, representing the distribution of the Fc head position above the electrode (more precisely above the thiol layer, see Supporting Information – Section 4). Heat maps simulated for Fc-dT_{35}, in its single and double stranded state, are shown in Figure 7a and 7b, respectively.

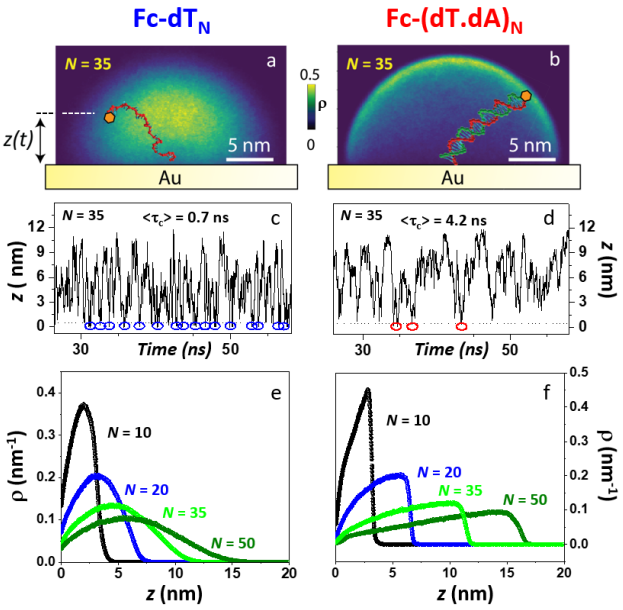

Figure 7. Molecular dynamics simulation of electrode end-attached Fc-dT strands. (Top panel) - Heat maps showing the distribution of the position of the ferrocene label in a plane perpendicular to the electrode surface and containing the chain anchoring point: (a) for Fc-dT_{35}, and, (b) for Fc-$(dT.dA)_{35}$. (Middle panel) - Time traces of the distance *z* separating the ferrocene head from the electrode surface: (c) for Fc-dT_{35}, (d) for Fc-$(dT.dA)_{35}$. Blue and red circles indicate "collision" events, defined as the ferrocene approaching the electrode surface within 0.1 nm. The average time separating two collisions $<t_c>$, derived from 10 μs long traces, is indicated. (Bottom panel) – Equilibrium distribution of the position the ferrocene above the electrode surface, derived for various chain lengths (*N*): (e) for Fc-dT_N, (f) for Fc-$(dT.dA)_N$.

As expected, a "mushroom" – shaped distribution is found for ssDNA and a hemispherical distribution for the rigid, rod like dsDNA. The instantaneous vertical position of Fc over the gold electrode interface, *z(t)*, is of particular interest here, and is monitored throughout the simulation time. Figures 7c and 7d show short samples of such time traces obtained for Fc-dT_{35} and Fc-$(dT.dA)_{35}$, respectively.

Numerous collisions of the Fc label with the electrode, defined by z< 1 Å, can be identified (blue and red circles). It is found that the average collision time $<\tau_c>$ is on the order of sub-ns for ssDNA and ns for dsDNA. Such very short collision times are due to confinement of the Fc-head motion to the immediate vicinity of the electrode, within a nanometer-scaled hemispherical region defined by the chain length. Similarly short collision times were obtained by White et al. from random walk simulations of the Brownian motion of a molecule confined to a hemispherical volume on an electrode.[24]

Most importantly, these collision times are several orders of magnitude shorter than the µs time scale one would predict from diffusion coefficients of the ss and dsDNA chains. This further supports our view of the motional dynamics of the Fc label being too fast to kinetically limit the electron transport in anchored DNA layers, and validates the use of the TLC model.

Averaging the time traces enables ρ(z), the equilibrium probability of finding the Fc label at a distance z from the electrode surface, to be derived. ρ(z) vs. z profiles simulated for Fc-dT_N chains of various lengths (N=10-50) are shown in Figure 7e and 7f, for ss and ds DNA, respectively. The profiles obtained for ssDNA are seen to be almost ideally Gaussian- shaped, as expected for a 1D elastico-diffusive motion,[59] whereas they display a more complex shape for dsDNA. The probability of finding the Fc-label *at the electrode surface*, $\rho_e = \rho(z=0)$, is particularly relevant for interpreting CV experiments. Figure 8 shows ρ_e values derived from the probability profiles presented in Figure 7.

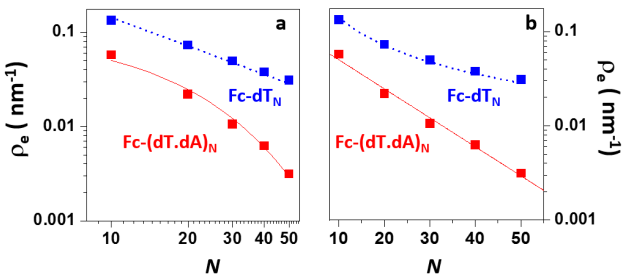

Figure 8. Molecular dynamics simulation of electrode end-attached Fc-$(dT)_N$ and Fc-$(dT.dA)_N$ strands. Equilibrium probability of presence of the Fc label at the electrode surface, ρ_e, as function of the DNA chain length (*N*). Log(ρ_e) is plotted versus: (a) Log(*N*), and, (b), *N*. Blue and red symbols correspond to Fc-$(dT)_N$ and Fc-$(dT.dA)_N$ data, respectively. The blue dotted lines in (a) and (b) are a plots of the equation: $\rho_e = 1/(0.7\times N)$. The red solid lines in (a) and (b) correspond to the exponential best-fit function for Fc-$(dT.dA)_N$ data: $\rho_e = 0.1 \times \exp(-N/14.1)$.

In the ssDNA case (blue symbols), a clear $1/N$ variation of ρ_e vs. *N* is seen, in agreement with the predictions of Plaxco et al. in their earlier works.[21] More quantitatively, we observed that ρ_e is accurately given by $\rho_e = 1/L_c$, where L_c is the contour length of the ssDNA chain, counting 0.7 nm per base (dashed blue line in Figure 8a and 8b). Hence, as far as its probability of presence at the electrode is concerned, the Fc head of Fc-ssDNA behaves similarly to a free species rapidly diffusing within a planar thin layer of thickness L_c.

In the Fc-dsDNA case (red symbols), a faster, approximately exponential decay of ρ_e with *N* is observed. These results illustrate that approaching the electrode is sterically "harder" for the Fc when the DNA strand is hybridized.

Discussion

Interpretation of the dependence of k_o on the DNA chain length (*N*), diluent length (*n*) and chain coverage (Γ)

In the framework of the MHL/TLC model used here, the rate of electron transfer is jointly modulated by the probability of the presence of the Fc head at the electron transfer site ρ(z), and by the rate of electron transfer between the redox probe and the electrode, $k_{ET}(z)$. Both quantities depend on *z*, the distance between the Fc head and the electrode. Hence the value of the overall rate of electron transfer, k_o, is given by integration over all possible transfer distances, ranging from the distance of closest approach, set by the thickness of the alkyl thiol layer, *d*, to infinity:

$$k_0 = \int_d^{+\infty} k_{ET}(z)\,\rho(z)dz \qquad (1)$$

$k_{ET}(z)$ decays exponentially with *z* as:

$$k_{ET}(z) = k_{ET}(z=0)\exp[-\beta z]$$

with a tunneling decay constant β ~1 $Å^{-1}$.

Equation (1) can be a priori calculated exactly, knowing ρ(z) from the simulations. It can also be simplified by noting that ρ(z) varies much slower with z than $k_{ET}(z)$, so that one can take $\rho(z)\sim\rho(z=0)$, i.e. one can solely consider the presence probability of the Fc head at the electrode surface, noted ρ_e. This yields:

$$k_0 = (k_{ET}(z=0)/\beta)\exp[-\beta d]\times\rho_e$$

$$= k_s\exp[-\beta d]\times\rho_e = k_s^d\times\rho_e \qquad (2)$$

where $k_s = k_{ET}(z=0)/\beta$ is the standard rate of heterogeneous electron transfer rate constant, familiar to the electrochemists and known for many redox species, and $k_s^d = k_s\exp[-\beta d]$. We verified that this approximation and full calculation of the integral equation (1) yielded identical theoretical k_o values, to within 40%. Equation (2) predicts that the value of k_o is jointly modulated by the intrinsic rate of the redox label electron transfer at a bare electrode (via k_s), the thickness of the alkyl-thiol (*d*) and the presence probability ρ_e (which notably depends on the chain length). The data presented herein enable us to assess the validity of these predictions.

Knowing ρ_e for any *N* value from our simulations, we fitted equation (2) to the experimental k_o vs. *N* variation for

Fc-$(dT)_N$, using k^d_s as a single adjustable parameter. The resulting best-fit curves, represented by red traces in Figure 5a and inset, reproduce the experimental data very satisfyingly, with the best fit value of k^d_s = (5.5 ± 0.5) ×10^{-3} cm/s. This value is very close to the k^d_s value of (3 ± 0.5) × 10^{-3} cm/s we measured in solution for ferrocenedimethanol, a good model of the DNA Fc label used here, at an MCH-coated gold electrode (see Figure S10). Similarly, the experimental k_o vs. N variation recorded for Fc-$(dT.dA)_N$ duplexes could be very satisfyingly reproduced on the basis of equation (2), using ρ_e values simulated for the duplexed chains, and the best fit value of k^d_s = (2.0 ± 0.5) × 10^{-3} cm/s (red trace in Figure 5c and inset). These results are very strong evidence that the CV response of both the ss and ds Fc-DNA chains is controlled by the equilibrium presence probability of the Fc head at the surface, which modulates the actual rate of electron transfer.

Another test of the validity of the above formalism is brought by analyzing the experimental dependence of k_o on the thiol-alkyl diluent length. Figure 6a and 6b show that, both for ss and dsDNA, k_o decayed exponentially with the diluent length (represented by n), as predicted by Equation (2). More quantitatively, linear regressions of the ln(k_o) vs. n data yielded a slope of - 0.95 ± 0.15 per CH_2 unit, both for ss and dsDNA layers. This value is in good agreement with the decay length of ~ - 1 ± 0.1 per CH_2 characteristic of tunneling processes through alkyl thiols. [49,51,60,61]

Finally, the fact that k_o was observed to decrease as the surface coverage, Γ, was raised (Figure 4) can simply be explained by the surface crowding lowering the probability of presence of the Fc head at the electrode.

The above results are thus strong quantitative evidence that the rate of electron transfer through the diluent layer kinetically controls the CV response of end anchored Fc-DNA chains.

These results also validate the use of the MHL/TLC model, complemented by OxDNA-based simulations to predict the electrochemical response of end-anchored Fc-ss and dsDNA chains.

Interpretation of the very low activation energy characterizing electron transfer of redox DNA

The unexpectedly low λ values measured here for ssDNA chains, and even more so for dsDNA chains, and their dependence on coverage, diluent, and chain length constitute an unprecedented finding for such systems. From a phenomenological point of view, such low λ values are found to be responsible for the decrease of *the intensity* of the CV signal of dsDNA at much lower scan rates than for ssDNA (Figure 2), i.e. for the "extinction" phenomena we reported very early-on for the CV response of end-attached Fc-DNA chains.[14,15]

Indeed, as illustrated here (see Supporting Information), the MHL/TLC model predicts that, for sufficiently low λ values, one can obtain broad bell-shaped $i_{pa}/\sqrt{v}$ vs. v variations, within an experimentally attainable range of scan rates. This range is dictated solely by the value of k_o and thus may correspond, for "slow" (low k_s) redox labels, to scan rates well within reach of commercial instrumentation. Therefore, we suspect that the peak or plateau-shaped $i_{pa}/\sqrt{v}$ vs. v variations, or equivalently the proportionality between i_{pa} and $\sqrt{v}$, often reported in CV studies of end-attached DNA (or PNA) chains, [15,16,20,23–26] actually reflect control of the electrochemical signal by the rate of electron transfer associated with a low λ value, rather than by chain dynamics.

Our simulations can bring some insights into the reason why mere attachment of the Fc head to a DNA chain, end-tethered to the surface, yields lower reorganization energies than typical of redox species free in solution. Two hypotheses can be proposed.

The first one is based on the observation that collision frequencies for Fc-DNA are much larger than what can be calculated for free Fc confined into a planar nanogap of a thickness comparable to the chain length, L_c. Indeed, in the latter case one would expect collision times in the order of $<\tau_c> \sim L_c^2/D$ = 100 ns, taking D =10^{-5} cm²/s, and L_c ~ 10 nm, i.e. a collision frequency two orders of magnitude lower than derived here for Fc-DNA.

Because of an increased collision frequency, it can be envisioned that the Fc head of DNA could, unlike free Fc, enter the Stern layer. The penetration of Fc in this electrostatic layer is to be understood in the framework of the collision theory, with Fc-DNA displacing adsorbed ions from the surface,[62,63] the displacement rate scaling with the collision frequency. Within the Stern layer, the Fc head would experience a static dielectric constant, ε_s, lower than in the bulk and approaching the value of the optical dielectric constant, ε_{opt} = 1.78.[64] The solvent reorganization energy, λ_o, would consequently decrease, as, at the electrode, it is given by:[33]

$$\lambda_0 = \frac{e^2}{8\pi\varepsilon_0}\left(\frac{1}{\varepsilon_{opt}} - \frac{1}{\varepsilon_s}\right)\frac{1}{2a_0} \qquad (3)$$

With ε_0 is the dielectric permittivity in vacuum, e the elementary charge and a_o = 0.38 nm the radius of Fc. Assuming ε_s ~ 2 in the Stern layer[65] would yield λ_o = 0.058 eV.

This effect would fall in line with the recent observation that redox molecules immobilized on an electrode, close enough to the surface to be located within the electric double layer, display greatly decreased λ_o values.[65]

The total reorganization energy, λ, determined here, is actually the sum of the solvent (λ_o) and internal (λ_i) reorganization energies:

$\lambda = \lambda_o + \lambda_i$

For ferrocene, λ_i was theoretically evaluated to ~0.016 eV.[66] Hence the above considerations would predict λ ~ 0.058 + 0.016 = 0.074 eV, which is close to the minimum value we found here for Fc-ssDNA. In that framework, the increase of λ with the surface coverage (Figure 4b) could be explained by a decrease of the collision frequency due do chain crowding. The modest variation of λ with the chain

length (Figure 5b) is also coherent with the weak dependence of the collision frequency with N as simulated (Figure S13). The expected independence of the collision frequency on the diluent length would also explain why λ was not found to be a function of n, (Figure 6b).

For Fc-dsDNA, the fact that we measured vanishingly small values of λ tends to show that λ_o was reduced to an even greater extent than for Fc-ssDNA, but also suggests that λ_i was reduced as well. This could be attributed to the rigidity of the dsDNA backbone and linker that limits the structural changes of the Fc head.[67] Just like for ssDNA, the experimental increase of λ with Γ is compatible with a negative correlation of λ with the collision frequency. The increase of λ with N (Figure 5d), and the fact that it is more pronounced than for ssDNA, parallel the simulated variation of the collision frequency with N (Figure S13).

The second hypothesis tentatively explaining the low λ values obtained for Fc-DNA is also based on a lower value of ε_s, but from a different origin, and is inspired by the studies of electrons transfer between redox centers in proteins. In these system, low λ values have been reported and explained by the very slow relaxation of water due to strong coupling of the redox species with slow parts of the system (here the coupling of Fc with DNA affecting water relaxation).[68]

Conclusions

We have demonstrated that, due to the intrinsically fast motional dynamics of oligonucleotides, the electrochemical response of end-attached, short, redox DNA strands is controlled by the rate of the electron transfer between the redox label and the electrode, even in the case of a "fast" redox mediator like ferrocene. As a result, the CV behavior of both ss and ds Fc-DNA chains can be fully and quantitatively described by the simple MHL/TLC model, in terms of only two parameters, k_o and λ . This can likely be generalized to any redox DNA system interrogated using any electrochemical technique. Moreover, the simulation package we have developed, by enabling the presence probability of the free end of the anchored DNA chains at the electrode surface to be calculated, can reliably predict the k_o value for any given end-grafted redox ss and ds-DNA system (of any sequence), provided the k_s value of the label is known independently.

We also revealed that the reorganization energy associated with the oxidation of the DNA-borne ferrocene label is significantly reduced as compared to free ferrocene in solution.

Our study also allowed us to demonstrate that the modulation of the electrochemical response of redox DNA strands induced by their hybridization can be fully explained by a variation of the parameters describing the electron transfer rate of the redox label (k_o, λ). The transition from single to double-stranded DNA is accompanied by a decrease in the probability of the presence of the redox label in the vicinity of the electrode, due to steric reasons, which results in a lower value of k_o. At the same time, and in a totally unexpected way, hybridization is associated with a significant decrease in the reorganization energy, which in some cases (i.e. diluted shorter chains) can reach values close to zero, strongly modifying the current response of the system.

The fact that λ values are found to be systematically lower for dsDNA than for ssDNA is the major factor rendering the electrochemical response of ss and dsDNA experimentally discernible from each other, much more than differences in k_o values. As such this phenomenon likely largely contributes to the signaling mechanism of E-DNA sensors.

ASSOCIATED CONTENT

Supporting Information. Material and methods section. Numerical calculation of the Fc-DNA CV wave using the MHL/TLC model. CV and AFM-SECM data evidencing the proper terminal self-assembly of Fc-dT layers. CV data showing the reversibility and specificity of the hybridization of surface attached Fc-dT20. Examples illustrating the good quality of fits of the MHL/TLC working curves to the CV data for various chain coverages, chain length, and alkyl diluents. Variation of k_o and λ parameters with the chain coverage for both Fc-dT_{20} and Fc-dT_{50} chains. CV determination of k^d_s for ferrocenedimethanol at a MCH coated TS-Au electrode. Description of the molecular dynamics simulation package. Dependence of the collision frequency of the Fc head on the DNA chain length. This material is available free of charge via the Internet at http://pubs.acs.org.

AUTHOR INFORMATION

Corresponding Author

* Christophe.demaille@u-paris.fr
* nclement@iis.u-tokyo.ac.jp

Author Contributions

The manuscript was written through contributions of all authors. All authors have given approval to the final version of the manuscript.

Funding Sources

This work has been supported by the the French “Agence Nationalede la Recherche”(ANR) through the “SIBI” pro-ject (ANR-19-CE42-0011-01).

ACKNOWLEDGMENT

This work has received financial support from the French “Agence Nationale de la Recherche” (ANR) through the “SIBI” project (ANR- 19-CE42-0011-01).

REFERENCES

(1) Lubin, A. A.; Plaxco, K. W. Folding-Based Electrochemical Biosensors: The Case for Responsive Nucleic Acid Architectures. *Acc. Chem. Res.* **2010**, *43* (4), 496–505. https://doi.org/10.1021/ar900165x.

(2) Du, Y.; Dong, S. Nucleic Acid Biosensors: Recent Advances and Perspectives. *Anal. Chem.* **2017**, *89* (1), 189–215. https://doi.org/10.1021/acs.analchem.6b04190.

(3) Ferapontova, E. E. DNA Electrochemistry and Electrochemical Sensors for Nucleic Acids. *Annu. Rev. Anal. Chem.* **2018**, *11* (1), 197–218. https://doi.org/10.1146/annurev-anchem-061417-125811.

(4) Ranallo, S.; Porchetta, A.; Ricci, F. DNA-Based Scaffolds for Sensing Applications. *Anal. Chem.* **2019**, *91* (1), 44–59. https://doi.org/10.1021/acs.analchem.8b05009.

(5) Pellitero, M. A.; Shaver, A.; Arroyo-Currás, N. Critical Review—Approaches for the Electrochemical Interrogation of DNA-Based Sensors: A Critical Review. *J. Electrochem. Soc.* **2019**, *167* (3), 37529. https://doi.org/10.1149/2.0292003jes.

(6) Arroyo-Currás, N.; Somerson, J.; Vieira, P. A.; Ploense, K. L.; Kippin, T. E.; Plaxco, K. W. Real-Time Measurement of Small Molecules Directly in Awake, Ambulatory Animals. *Proc. Natl. Acad. Sci.* **2017**, *114* (4), 645–650. https://doi.org/10.1073/pnas.1613458114.

(7) Xiao, Y.; Lubin, A. A.; Heeger, A. J.; Plaxco, K. W. Label-Free Electronic Detection of Thrombin in Blood Serum by Using an Aptamer-Based Sensor. *Angew. Chemie Int. Ed.* **2005**, *44* (34), 5456–5459. https://doi.org/https://doi.org/10.1002/anie.200500989.

(8) Yousefi, H.; Mahmud, A.; Chang, D.; Das, J.; Gomis, S.; Chen, J. B.; Wang, H.; Been, T.; Yip, L.; Coomes, E.; Li, Z.; Mubareka, S.; McGeer, A.; Christie, N.; Gray-Owen, S.; Cochrane, A.; Rini, J. M.; Sargent, E. H.; Kelley, S. O. Detection of SARS-CoV-2 Viral Particles Using Direct, Reagent-Free Electrochemical Sensing. *J. Am. Chem. Soc.* **2021**, *143* (4), 1722–1727. https://doi.org/10.1021/jacs.0c10810.

(9) Liu, J.; Zhou, H.; Xu, J.-J.; Chen, H.-Y. An Effective DNA-Based Electrochemical Switch for Reagentless Detection of Living Cells. *Chem. Commun.* **2011**, *47* (15), 4388–4390. https://doi.org/10.1039/C1CC10430F.

(10) Grall, S.; Li, S.; Jalabert, L.; Kim, S.-H.; Chovin, A.; Demaille, C.; Clement, N. *Electrochemical Shot-Noise of a Redox Monolayer*; arXiv, 2022. https://doi.org/10.48550/ARXIV.2210.12943.

(11) Gorodetsky, A. A.; Green, O.; Yavin, E.; Barton, J. K. Coupling into the Base Pair Stack Is Necessary for DNA-Mediated Electrochemistry. *Bioconjug. Chem.* **2007**, *18* (5), 1434–1441. https://doi.org/10.1021/bc0700483.

(12) Gupta, N. K.; Wilkinson, E. A.; Karuppannan, S. K.; Bailey, L.; Vilan, A.; Zhang, Z.; Qi, D. C.; Tadich, A.; Tuite, E. M.; Pike, A. R.; Tucker, J. H. R.; Nijhuis, C. A. Role of Order in the Mechanism of Charge Transport across Single-Stranded and Double-Stranded DNA Monolayers in Tunnel Junctions. *J. Am. Chem. Soc.* **2021**, *143* (48), 20309–20319. https://doi.org/10.1021/jacs.1c09549.

(13) Wierzbinski, E.; De Leon, A.; Yin, X.; Balaeff, A.; Davis, K. L.; Reppireddy, S.; Venkatramani, R.; Keinan, S.; Ly, D. H.; Madrid, M.; Beratan, D. N.; Achim, C.; Waldeck, D. H. Effect of Backbone Flexibility on Charge Transfer Rates in Peptide Nucleic Acid Duplexes. *J. Am. Chem. Soc.* **2012**, *134* (22), 9335–9342. https://doi.org/10.1021/ja301677z.

(14) Anne, A.; Bouchardon, A.; Moiroux, J. 3′-Ferrocene-Labeled Oligonucleotide Chains End-Tethered to Gold Electrode Surfaces: Novel Model Systems for Exploring Flexibility of Short DNA Using Cyclic Voltammetry. *J. Am. Chem. Soc.* **2003**, *125* (5), 1112–1113. https://doi.org/10.1021/ja028640k.

(15) Anne, A.; Demaille, C. Dynamics of Electron Transport by Elastic Bending of Short DNA Duplexes. Experimental Study and Quantitative Modeling of the Cyclic Voltammetric Behavior of 3′-Ferrocenyl DNA End-Grafted on Gold. *J. Am. Chem. Soc.* **2006**, *128*, 542–557. https://doi.org/10.1021/ja055112a.

(16) Anne, A.; Demaille, C. Electron Transport by Molecular Motion of Redox-DNA Strands: Unexpectedly Slow Rotational Dynamics of 20-Mer Ds-DNA Chains End-Grafted onto Surfaces via C6 Linkers. *J. Am. Chem. Soc.* **2008**, *130* (30), 9812–9823. https://doi.org/10.1021/ja801074m.

(17) Ricci, F.; Lai, R. Y.; Plaxco, K. W. Linear, Redox Modified DNA Probes as Electrochemical DNA Sensors. *Chem. Commun.* **2007**, No. 36, 3768–3770. https://doi.org/10.1039/B708882E.

(18) Xiao, Y.; Uzawa, T.; White, R. J.; DeMartini, D.; Plaxco, K. W. On the Signaling of Electrochemical Aptamer-Based Sensors: Collision- and Folding-Based Mechanisms. *Electroanalysis* **2009**, *21* (11), 1267–1271. https://doi.org/https://doi.org/10.1002/elan.200804564.

(19) Uzawa, T.; Cheng, R. R.; White, R. J.; Makarov, D. E.; Plaxco, K. W. A Mechanistic Study of Electron Transfer from the Distal Termini of Electrode-Bound, Single-Stranded DNAs. *J. Am. Chem. Soc.* **2010**, *132* (45), 16120–16126. https://doi.org/10.1021/ja106345d.

(20) Abi, A.; Ferapontova, E. E. Unmediated by DNA Electron Transfer in Redox-Labeled DNA Duplexes End-Tethered to Gold Electrodes. *J. Am. Chem. Soc.* **2012**, *134* (35), 14499–14507. https://doi.org/10.1021/ja304864w.

(21) Dauphin-Ducharme, P.; Arroyo-Currás, N.; Adhikari, R.; Somerson, J.; Ortega, G.; Makarov, D. E.; Plaxco, K. W. Chain Dynamics Limit Electron Transfer from Electrode-Bound, Single-Stranded Oligonucleotides. *J. Phys. Chem. C* **2018**, *122* (37), 21441–21448. https://doi.org/10.1021/acs.jpcc.8b06111.

(22) Dauphin-Ducharme, P.; Arroyo-Currás, N.; Plaxco, K. W. High-Precision Electrochemical Measurements of the Guanine-, Mismatch-, and Length-Dependence of Electron Transfer from Electrode-Bound DNA Are Consistent with a Contact-Mediated Mechanism. *J. Am. Chem. Soc.* **2019**, *141* (3), 1304–1311. https://doi.org/10.1021/jacs.8b11341.

(23) Farjami, E.; Campos, R.; Ferapontova, E. E. Effect of the DNA End of Tethering to Electrodes on Electron Transfer in Methylene Blue-Labeled DNA Duplexes. *Langmuir* **2012**, *28* (46), 16218–16226. https://doi.org/10.1021/la3032336.

(24) Huang, K. C.; White, R. J. Random Walk on a Leash: A Simple Single-Molecule Diffusion Model for Surface-Tethered Redox Molecules with Flexible Linkers. *J. Am. Chem. Soc.* **2013**, *135* (34), 12808–12817. https://doi.org/10.1021/ja4060788.

(25) Hüsken, N.; Gębala, M.; La Mantia, F.; Schuhmann, W.; Metzler-Nolte, N. Mechanistic Studies of Fc-PNA(·DNA) Surface Dynamics Based on the Kinetics of Electron-Transfer Processes. *Chem. – A Eur. J.* **2011**, *17* (35), 9678–9690. https://doi.org/https://doi.org/10.1002/chem.201003764.

(26) Hüsken, N.; Gębala, M.; Battistel, A.; La Mantia, F.; Schuhmann, W.; Metzler-Nolte, N. Impact of Single Basepair Mismatches on Electron-Transfer Processes at Fc-PNA·DNA Modified Gold Surfaces. *ChemPhysChem* **2012**, *13* (1), 131–139. https://doi.org/https://doi.org/10.1002/cphc.201100578.

(27) Stellwagen, N. C.; Magnusdottir, S.; Gelfi, C.; Righetti, P. G. Measuring the Translational Diffusion Coefficients of Small DNA Molecules by Capillary Electrophoresis. *Biopolymers* **2001**, *58* (4), 390–397. https://doi.org/https://doi.org/10.1002/1097-0282(20010405)58:4<390::AID-BIP1015>3.0.CO;2-K.

(28) Ortega, A.; Garcia De La Torre, J. Hydrodynamic Properties of Rodlike and Dislike Particles in Dilute Solution. *J. Chem. Phys.* **2003**, *119* (18), 9914–9919. https://doi.org/10.1063/1.1615967.

(29) Langer, A.; Kaiser, W.; Svejda, M.; Schwertler, P.; Rant, U. Molecular Dynamics of DNA-Protein Conjugates on Electrified Surfaces: Solutions to the Drift-Diffusion Equation. *J. Phys. Chem. B* **2014**, *118* (2), 597–607. https://doi.org/10.1021/jp410640z.

(30) Rant, U.; Arinaga, K.; Tornow, M.; Yong, W. K.; Netz, R. R.; Fujita, S.; Yokoyama, N.; Abstreiter, G. Dissimilar Kinetic Behavior of Electrically Manipulated Single- and Double-Stranded DNA Tethered to a Gold Surface. *Biophys. J.* **2006**, *90* (10), 3666–3671. https://doi.org/10.1529/biophysj.105.078857.

(31) Jähner, S.; Hampel, P. A.; Langer, A.; Maruyama, M.; Kaiser, W.; Rant, U.; Welte, T.; Knezevic, J.; Strasser, R.; Svejda, M.; Villa, V.; Fischer, F. Protein Analysis by Time-Resolved Measurements with an Electro-Switchable DNA Chip. *Nat. Commun.* **2013**, *4* (1), 2099. https://doi.org/10.1038/ncomms3099.

(32) Snodin, B. E. K.; Randisi, F.; Mosayebi, M.; Šulc, P.; Schreck, J. S.; Romano, F.; Ouldridge, T. E.; Tsukanov, R.; Nir, E.; Louis, A. A.; Doye, J. P. K. Introducing Improved Structural Properties and Salt Dependence into a Coarse-Grained Model of DNA. *J. Chem. Phys.* **2015**, *142* (23), 234901. https://doi.org/10.1063/1.4921957.

(33) Marcus, R. A. On the Theory of Electron-Transfer Reactions. VI. Unified Treatment for Homogeneous and Electrode Reactions. *J. Chem. Phys.* **1965**, *43* (2), 679–701. https://doi.org/10.1063/1.1696792.

(34) Chidsey, C. E. D. Free Energy and Temperature Dependence of Electron Transfer at the Metal-Electrolyte Interface. *Science (80-.).* **1991**, *4996* (251), 919–922. https://doi.org/10.1126/science.251.4996.919.

(35) Savéant, J.-M. Effect of the Electrode Continuum of States in Adiabatic and Nonadiabatic Outer-Sphere and Dissociative Electron Transfers. Use of Cyclic Voltammetry for Investigating Nonlinear Activation-Driving Force Laws. *J. Phys. Chem. B* **2002**, *106* (36), 9387–9395. https://doi.org/10.1021/jp0258006.

(36) Mahlum, J. D.; Pellitero, M. A.; Arroyo-Currás, N. Chemical Equilibrium-Based Mechanism for the Electrochemical Reduction of DNA-Bound Methylene Blue Explains Double Redox Waves in Voltammetry. *J. Phys. Chem. C* **2021**, *125* (17), 9038–9049. https://doi.org/10.1021/acs.jpcc.1c00336.

(37) Levicky, R.; Herne, T. M.; Tarlov, M. J.; Satija, S. K. Using Self-Assembly To Control the Structure of DNA Monolayers on Gold: A Neutron Reflectivity Study. *J. Am. Chem. Soc.* **1998**, *120* (38), 9787–9792. https://doi.org/10.1021/ja981897r.

(38) Meunier, A.; Triffaux, E.; Bizzotto, D.; Buess-Herman, C.; Doneux, T. In Situ Fluorescence Microscopy Study of the Interfacial Inhomogeneity of DNA Mixed Self-Assembled Monolayers at Gold Electrodes. *ChemElectroChem* **2015**, *2* (3), 434–442. https://doi.org/https://doi.org/10.1002/celc.201402273.

(39) Doneux, T.; De Rache, A.; Triffaux, E.; Meunier, A.; Steichen, M.; Buess-Herman, C. Optimization of the Probe Coverage in DNA Biosensors by a One-Step Coadsorption Procedure. *ChemElectroChem* **2014**, *1* (1), 147–157. https://doi.org/https://doi.org/10.1002/celc.201300145.

(40) Wang, K.; Goyer, C.; Anne, A.; Demaille, C. Exploring the Motional Dynamics of End-Grafted DNA Oligonucleotides by in Situ Electrochemical Atomic Force Microscopy. *J. Phys. Chem. B* **2007**, *111*, 6051–6058. https://doi.org/10.1021/jp070432x.

(41) Kaiser, W.; Rant, U. Conformations of End-Tethered DNA Molecules on Gold Surfaces: Influences of Applied Electric Potential, Electrolyte Screening, and Temperature. *J. Am. Chem. Soc.* **2010**, *132* (23), 7935–7945. https://doi.org/10.1021/ja9087527d.

(42) Ge, D.; Levicky, R. A Comparison of Five Bioconjugatable Ferrocenes for Labeling of Biomolecules. *Chem. Commun.* **2010**, *46* (38), 7190–7192. https://doi.org/10.1039/CoCC02044C.

(43) Hubbard, T.; Anson, F. C. The Theory and Practice of Electrochemistry with Thin Layer Cells. In *Electroanalytical Chemistry: A Series of Advances*; 1970; pp 129–214.

(44) Laviron, E. General Expression of the Linear Potential Sweep Voltammogram in the Case of Diffusionless Electrochemical Systems. *J. Electroanal. Chem.* **1979**, *101*, 19–28. https://doi.org/10.1016/S0022-0728(79)80075-3.

(45) Marcus, R. A. On the Theory of Electron-Transfer Reactions. VI. Unified Treatment for Homogeneous and Electrode Reactions. *J. Chem. Phys.* **1965**, *43* (2), 679–701. https://doi.org/10.1063/1.1696792.

(46) Savéant, J.-M. Effect of the Electrode Continuum of States in Adiabatic and Nonadiabatic Outer-Sphere and Dissociative Electron Transfers. Use of Cyclic Voltammetry for Investigating Nonlinear Activation-Driving Force Laws. *J. Phys. Chem. B* **2002**, *106* (36), 9387–9395. https://doi.org/10.1021/jp0258006.

(47) Weber, K.; Creager, S. E. Voltammetry of Redox-Active Groups Irreversibly Adsorbed onto Electrodes. Treatment Using the Marcus Relation between Rate and Overpotential. *Anal. Chem.* **1994**, *66* (19), 3164–3172. https://doi.org/10.1021/ac00091a027.

(48) Nahir, T. M.; Clark, R. A.; Bowden, E. F. Linear-Sweep Voltammetry of Irreversible Electron Transfer in Surface-Confined Species Using the Marcus Theory. *Anal. Chem.* **1994**, *66* (15), 2595–2598. https://doi.org/10.1021/ac000087a027.

(49) Smalley, J. F.; Feldberg, S. W.; Chidsey, C. E. D.; Linford, M. R.; Newton, M. D.; Liu, Y.-P. The Kinetics of Electron Transfer Through Ferrocene-Terminated Alkanethiol Monolayers on Gold. *J. Phys. Chem.* **1995**, *99* (35), 13141–13149. https://doi.org/10.1021/j100035a016.

(50) Richardson, J. N.; Peck, S. R.; Curtin, L. S.; Tender, L. M.; Terrill, R. H.; Carter, M. T.; Murray, R. W.; Rowe, G. K.; Creager, S. E. Electron-Transfer Kinetics of Self-Assembled Ferrocene Octanethiol Monolayers on Gold and Silver Electrodes from 115 to 170 K. *J. Phys. Chem.* **1995**, *99* (2), 766–772. https://doi.org/10.1021/j100002a046.

(51) Smalley, J. F.; Finklea, H. O.; Chidsey, C. E. D.; Linford, M. R.; Creager, S. E.; Ferraris, J. P.; Chalfant, K.; Zawodzinsk, T.; Feldberg, S. W.; Newton, M. D. Heterogeneous Electron-Transfer Kinetics for Ruthenium and Ferrocene Redox Moieties through Alkanethiol Monolayers on Gold. *J. Am. Chem. Soc.* **2003**, *125* (7), 2004–2013. https://doi.org/10.1021/ja028458j.

(52) Kang, D.; Zuo, X.; Yang, R.; Xia, F.; Plaxco, K. W.; White, R. J. Comparing the Properties of Electrochemical-Based DNA Sensors Employing Different Redox Tags. *Anal. Chem.* **2009**, *81* (21), 9109–9113. https://doi.org/10.1021/ac9018111n.

(53) Chi, Q.; Wang, G.; Jiang, J. The Persistence Length and Length per Base of Single-Stranded DNA Obtained from Fluorescence Correlation Spectroscopy Measurements Using Mean Field Theory. *Phys. A Stat. Mech. its Appl.* **2013**, *392* (5), 1072–1079. https://doi.org/https://doi.org/10.1016/j.physa.2012.09.022.

(54) Sinden, R. R. CHAPTER 1 - Introduction to the Structure, Properties, and Reactions of DNA; Sinden, R. R. B. T.-D. N. A. S. and F., Ed.; Academic Press: San Diego, 1994; pp 1–57. https://doi.org/https://doi.org/10.1016/B978-0-08-057173-7.50006-7.

(55) Bond, A. M.; Colton, R.; Harvey, J.; Hutton, R. S. Voltammetric Studies of Ferrocene and the Mercury Dithiophosphate System at Mercury Electrodes over a Temperature Range Encompassing the Mercury Liquid-Solid State Transition. *J. Electroanal. Chem.* **1997**, *426* (1), 145–155. https://doi.org/https://doi.org/10.1016/S0022-0728(96)04969-8.

(56) Yang, W.; Lai, R. Y. Effect of Diluent Chain Length on the Performance of the Electrochemical DNA Sensor at Elevated Temperature. *Analyst* **2011**, *136* (1), 134–139.

https://doi.org/10.1039/CoANoo644K.
(57) Ricci, F.; Zari, N.; Caprio, F.; Recine, S.; Amine, A.; Moscone, D.; Palleschi, G.; Plaxco, K. W. Surface Chemistry Effects on the Performance of an Electrochemical DNA Sensor. *Bioelectrochemistry* **2009**, *76* (1), 208–213. https://doi.org/https://doi.org/10.1016/j.bioelechem.2009.03.007.
(58) Das, J.; Gomis, S.; Chen, J. B.; Yousefi, H.; Ahmed, S.; Mahmud, A.; Zhou, W.; Sargent, E. H.; Kelley, S. O. Reagentless Biomolecular Analysis Using a Molecular Pendulum. *Nat. Chem.* **2021**, *13* (5), 428–434. https://doi.org/10.1038/s41557-021-00644-y.
(59) Anne, A.; Demaille, C.; Moiroux, J. Elastic Bounded Diffusion. Dynamics of Ferrocene-Labeled Poly(Ethylene Glycol) Chains Terminally Attached to the Outermost Monolayer of Successively Self-Assembled Monolayers of Immunoglobulins. *J. Am. Chem. Soc.* **1999**, *121*, 10379–10388. https://doi.org/10.1021/ja991780i.
(60) Finklea, H. O.; Hanshew, D. D. Electron-Transfer Kinetics in Organized Thiol Monolayers with Attached Pentaammine(Pyridine)Ruthenium Redox Centers. *J. Am. Chem. Soc.* **1992**, *114* (9), 3173–3181. https://doi.org/10.1021/ja00035a001.
(61) Slowinski, K.; Slowinska, K. U.; Majda, M. Electron Tunneling Across Hexadecanethiolate Monolayers on Mercury Electrodes: Reorganization Energy, Structure, and Permeability of the Alkane/Water Interface. *J. Phys. Chem. B* **1999**, *103* (40), 8544–8551. https://doi.org/10.1021/jp991466a.
(62) Horinek, D.; Netz, R. R. Specific Ion Adsorption at Hydrophobic Solid Surfaces. *Phys. Rev. Lett.* **2007**, *99* (22), 226104. https://doi.org/10.1103/PhysRevLett.99.226104.
(63) Sivakumarasamy, R.; Hartkamp, R.; Siboulet, B.; Dufrêche, J.-F.; Nishiguchi, K.; Fujiwara, A.; Clément, N. Selective Layer-Free Blood Serum Ionogram Based on Ion-Specific Interactions with a Nanotransistor. *Nat. Mater.* **2018**, *17*, 464–470. https://doi.org/10.1038/s41563-017-0016-y.
(64) Bonthuis, D. J.; Gekle, S.; Netz, R. R. Dielectric Profile of Interfacial Water and Its Effect on Double-Layer Capacitance. *Phys. Rev. Lett.* **2011**, *107* (16), 166102. https://doi.org/10.1103/PhysRevLett.107.166102.
(65) Bangle, R. E.; Schneider, J.; Conroy, D. T.; Aramburu-Trošelj, B. M.; Meyer, G. J. Kinetic Evidence That the Solvent Barrier for Electron Transfer Is Absent in the Electric Double Layer. *J. Am. Chem. Soc.* **2020**, *142* (35), 14940–14946. https://doi.org/10.1021/jacs.0c05226.
(66) Paul, A.; Borrelli, R.; Bouyanfif, H.; Gottis, S.; Sauvage, F. Tunable Redox Potential, Optical Properties, and Enhanced Stability of Modified Ferrocene-Based Complexes. *ACS Omega* **2019**, *4* (12), 14780–14789. https://doi.org/10.1021/acsomega.9b01341.
(67) Gray, H. B.; Malmström, B. G.; Williams, R. J. P. Copper Coordination in Blue Proteins. *JBIC J. Biol. Inorg. Chem.* **2000**, 5 (5), 551–559. https://doi.org/10.1007/s007750000146.
(68) Martin, D. R.; Matyushov, D. V. Communication: Microsecond Dynamics of the Protein and Water Affect Electron Transfer in a Bacterial Bc1 Complex. *J. Chem. Phys.* **2015**, *142* (16), 161101. https://doi.org/10.1063/1.4919222.

Table of Contents Graphics